# Analysis of Electromagnetic Wave Propagation in Variable Magnetized Plasma via Polynomial Chaos Expansion

Bach T. Nguyen, Alireza Samimi, Stephen E. Wiechecki Vergara, *Member, IEEE*, Costas D. Sarris, *Senior Member, IEEE*, and Jamesina J. Simpson, *Senior Member, IEEE*

***Abstract*— A 3-D stochastic finite-difference time-domain algorithm is developed and applied to electromagnetic (EM) wave propagation in collisional magnetized plasma characterized by a variable electron density, collision frequency, and background magnetic field. The proposed stochastic model is based on the expansion of the random/variable time-domain electric and magnetic fields in terms of orthogonal polynomials in independent random variables representative of the variable ionospheric content. EM wave propagation in magnetized plasma having low variability (small deviations) and also high variability (large deviations) of the electron density, collision frequency, and background magnetic field is studied. The stochastic algorithm is validated against brute-force Monte Carlo results. The algorithm is considerably more computationally efficient than Monte Carlo. When applied to EM wave propagation in the ionosphere, the variability of the Earth's magnetic field and ionospheric parameters can be accounted for due to naturally varying space weather conditions and day-to-day variations, measurement errors, and so on. Although only electrons are considered here, positive and negative ions may be accommodated in a straightforward manner.**

***Index Terms*— Collisional magnetized cold plasma, electromagnetic (EM) wave propagation, finite-difference time-domain (FDTD), ionosphere, polynomial chaos, uncertainty.**

## I. Introduction

THE finite-difference time-domain (FDTD) method [1], [2] is a robust numerical modeling approach that has been widely utilized to solve for electromagnetic (EM) wave propagation in the Earth-ionosphere waveguide (e.g., [3]–[11]). Initially, 2-D "moving window" FDTD models were developed in [3] and [4]. More recently, fully 3-D global FDTD models of the Earth-ionosphere waveguide were generated that account for the anisotropic magnetized ionospheric plasma [11]. Specifically, a fully 3-D Cartesian plasma model developed in [12] was applied to the 3-D FDTD latitude–longitude global spherical grid [11] in [5]. By accounting for 3-D magnetized ionospheric plasma physics, [12] was the first global FDTD model to include the calculation of all important ionospheric effects on signals, including refraction, absorption, frequency shift, phase and group delay, polarization, and Faraday rotation. Subsequently, a more efficient magnetized plasma algorithm which avoids the complex matrix formulation used in [11] was published and adapted to the 3-D FDTD latitude–longitude global model [13].

All of the above 2-D and 3-D FDTD plasma models, however, account for only average (mean) composition values of the lithosphere and ionosphere and then solve for only expected (mean) electric and magnetic fields without considering the associated uncertainties in these physical quantities. One exception is Reference [14], in which a stochastic FDTD model of the global Earth-ionosphere waveguide is generated, however, it assumes an isotropic ionospheric plasma which may only be used at extremely low frequencies and below. Not accounting for the magnetized ionospheric plasma as well as the variability of the lithosphere and ionosphere content can limit the utility of EM propagation modeling for communications, surveillance, navigation, and geophysical applications. As one example, the ionosphere strongly effects transionospheric EM propagation: the irregularities in the electron density distribution can cause highly complex phase and amplitude scintillation. In these situations, it is highly desirable to consider models which account for random variability within the propagation media.

To account for the the variable/uncertain composition and dynamics resulting from solar and geomagnetic activities, the ionosphere may be treated as a random medium. Past and recent investigations (see [15]–[22]) on the temporal and spatial ionospheric variations have improved our understanding of the dynamics of the ionosphere under normal and disturbed conditions. This knowledge should be incorporated into numerical EM propagation models. The brute-force Monte Carlo method could be used, but it is computationally expensive, and quickly becomes computationally infeasible for 3-D problems.

Manuscript received August 28, 2017; revised August 22, 2018; accepted September 28, 2018. Date of publication November 5, 2018; date of current version January 16, 2019. This work was supported in part by the U.S. Air Force, in part by the Blue Waters Sustained Petascale Computing Project under Award #1440023, in part by the National Science Foundation under Award OCI-0725070 and Award ACI-1238993, and in part by the State of Illinois. *(Corresponding author: Bach T. Nguyen.)*

B. T. Nguyen and J. J. Simpson are with the Department of Electrical and Computer Engineering, University of Utah, Salt Lake City, UT 84112 USA (e-mail: bach.nguyen@utah.edu).

A. Samimi is with Nanometrics Inc., Milpitas, CA 95035 USA.

S. E. W. Vergara is with Vencore Inc., Melbourne, FL 32940 USA.

C. D. Sarris is with the Department of Electrical and Computer Engineering, University of Toronto, Toronto, ON M5S 3G4, Canada.

Color versions of one or more of the figures in this paper are available online at http://ieeexplore.ieee.org.

Digital Object Identifier 10.1109/TAP.2018.2879676

To overcome this problem, stochastic FDTD (S-FDTD) was proposed [23]. The advantage of the S-FDTD plasma algorithm is that it provides a direct estimate of both the mean and variance of the EM fields within a variable ionosphere at every point in space and time, while requiring only about twice as much computer simulation time and memory. However, its accuracy is limited by the fact that it requires estimates for the cross-correlation coefficients of the plasma frequency and the electric fields. A good procedure for determining the best estimates for these cross correlations is not yet known. Moreover, the Taylor series truncations may lead to insufficient accuracy in some cases.

This paper presents an alternative approach to S-FDTD and instead uses the spectral expansion or polynomial chaos expansion (PCE) method [24], [25] to represent the stochastic variability of the EM wave propagation in the magnetized cold plasma medium model. Polynomial chaos has previously been applied to computational fluid dynamics [26], [27] and some specific computational EM problems (see [28]–[37]). PCE is a robust method based on the expansion of the random output quantities of interest into a sum of a limited number of orthogonal polynomials of random input variables. It is versatile in that it can be applied to non-Gaussian problems, and its accuracy may be improved by simply increasing the order of the orthogonal polynomials. Recently, the PCE method was applied to investigate the impact of fire on the indoor wireless channel where fire is modeled as a cold plasma medium without considering the ambient magnetic field **B** (i.e., isotropic unmagnetized plasma) [38].

Here, we apply the PCE method to EM propagation in the ionosphere in the presence of a magnetic field, **B**. Specifically, realistic ionospheric electron densities and collision frequencies are used, but the ambient **B** is stronger than the Earth's actual magnetic field so that it will alter particle trajectories over a relatively short distance (i.e., behave as an anisotropic magnetized plasma). Using a larger **B** allows the use of smaller FDTD grids, which makes a comparison with Monte Carlo results more feasible.

In considering the variability of the ionosphere content, **B** is also treated as a 3-D random parameter since the Earth's magnetic field changes over time. The variation of **B** arises from the variation of currents in the ionosphere and magnetosphere or from the motion of molten iron alloys in its outer core. Our ultimate objective is to develop an optimal (efficient and accurate) stochastic FDTD-based algorithm that is well suited for large uncertainty quantification of the ionosphere and Earth's magnetic field. Note that relative to [39], this paper addresses collisional plasma (versus collisionless plasma), addresses the multivariable case (versus the univariate case), and provides significantly more details/results such that others may better understand and replicate our work as needed. Finally, although only electrons are considered in this paper, the PCE formulation presented here is identical for handling positive or negative ions as well.

## II. Formulation

This section presents the primary relevant aspects of the magnetized collisional ionospheric plasma algorithm of [13] (presented in Section II-A) that are needed to understand the PCE magnetized plasma formulation (presented in Section II-B). Finally, the methodology for calculating the global sensitivities of each input parameter on the EM fields is provided in Section II-C.

### *A. 3-D FDTD Collisional Magnetized Plasma Formulation*

Plasma in the presence of an ambient magnetic field, for example, the ionosphere in the presence of the Earth's magnetic field, becomes an anisotropic medium. The governing equation set is comprised of Maxwell's curl equations and the Lorentz force equation as follows:

$$\nabla \times \mathbf{E} = -\mu_0 \frac{\partial \mathbf{H}}{\partial t} \tag{1}$$

$$\nabla \times \mathbf{H} = \epsilon_0 \frac{\partial \mathbf{E}}{\partial t} + \mathbf{J}_e \tag{2}$$

$$\frac{\partial \mathbf{J}_e}{\partial t} + \upsilon_e \mathbf{J}_e = \epsilon_0 \omega_{Pe}^2 \mathbf{E} + \boldsymbol{\omega}_{Ce} \times \mathbf{J}_e \tag{3}$$

where $J_e$ is the electron current density and $\upsilon_e$ (the electron collision frequency), $\boldsymbol{\omega}_{Ce}$ (the electron cyclotron frequency), and $\omega_{Pe}$ (the electron plasma frequency) are fundamental plasma parameters which define various characteristics of a plasma. The plasma frequency may be calculated via the electron density $n_e$ as follows:

$$\omega_{Pe} = \sqrt{\frac{q_e^2 n_e}{\epsilon_0 m_e}}. \tag{4}$$

The electron cyclotron frequency is a function of the applied magnetic field **B** as follows: $\boldsymbol{\omega}_{Ce} = |q_e|\mathbf{B}/m_e$.

By taking advantages of the Boris algorithm (which has been widely applied to particle-in-cell plasma modeling [40], [41]) and the MacCormack predictor–corrector method [42], [43], [13] provides an efficient 3-D FDTD magnetized plasma algorithm in which the Lorentz equation is derived explicitly and incorporated into the traditional FDTD Maxwell's equations [e.g., the $x$-component equations are provided in (5)–(8), as shown at the top of the next page]. Now, the Lorentz equation involves a predicted current density vector $\mathbf{J}_{e,p}$ and a corrected current density vector $\mathbf{J}_{e,c}$, where $\theta$ is an angle between two auxiliary current density vectors $\mathbf{J}^+$ and $\mathbf{J}^-$ via Boris scheme. Then, the final current density vector is the average of the predicted current density vector and the corrected current density vector. Fig. 1 illustrates the positions of the EM field and current density components in the Yee cell, where all of the current density components are solved at the position of $E_x$. More details on this algorithm may be found in [13]. In this paper, we have applied a simple PEC boundary condition at all of the boundaries, and have used a sufficiently large computational grid to avoid any reflections from the boundaries over the time span of interest. A more suitable boundary condition that accounts for the plasma as well as the uncertainty is challenging and beyond the scope of this paper. It will be important for follow-on work.

### *B. 3-D-PCE-FDTD Collisional Magnetized Plasma Formulation*

The ionosphere exhibits large variations in both time and space. Previous studies showed that the ionosphere content,

*Regular H-Field Update*:

$$H_x\big|_{i,j+1/2,k+1/2}^{n+1/2} = H_x\big|_{i,j+1/2,k+1/2}^{n-1/2} + \frac{\Delta t}{\mu_0}\left[\frac{E_y\big|_{i,j+1/2,k+1}^{n} - E_y\big|_{i,j+1/2,k}^{n}}{\Delta z} - \frac{E_z\big|_{i,j+1,k+1/2}^{n} - E_z\big|_{i,j,k+1/2}^{n}}{\Delta y}\right]. \tag{5}$$

*For the Predictor Step*:

$$\begin{aligned}
&J_{ex,p}\big|_{i+1/2,j,k}^{n+1/2} \\
&\quad= J_{ex}\big|_{i+1/2,j,k}^{n-1/2} + \Delta t\epsilon_0\omega_{Pe}^2 E_x\big|_{i+1/2,j,k}^{n} - \Delta t v_e J_{ex}\big|_{i+1/2,j,k}^{n-1/2} - \frac{\sin\theta}{|\omega_{Ce}|}\left(J_{ey}\big|_{i+1/2,j,k}^{n-1/2}\omega_{Cez} - J_{ez}\big|_{i+1/2,j,k}^{n-1/2}\omega_{Cey}\right) \\
&\qquad- \frac{\Delta t\epsilon_0\sin\theta}{2|\omega_{Ce}|}\omega_{Pe}^2\left(E_y\big|_{i+1/2,j,k}^{n}\omega_{Cez} - E_z\big|_{i+1/2,j,k}^{n}\omega_{Cey}\right) + \frac{\Delta t\sin\theta}{2|\omega_{Ce}|}v_e\left(J_{ey}\big|_{i+1/2,j,k}^{n-1/2}\omega_{Cez} - J_{ez}\big|_{i+1/2,j,k}^{n-1/2}\omega_{Cey}\right) \\
&\qquad+ \frac{\tan\frac{\theta}{2}\sin\theta}{|\omega_{Ce}|^2}\left[\left(J_{ez}\big|_{i+1/2,j,k}^{n-1/2}\omega_{Cex} - J_{ex}\big|_{i+1/2,j,k}^{n-1/2}\omega_{Cez}\right)\omega_{Cez} - \left(J_{ex}\big|_{i+1/2,j,k}^{n-1/2}\omega_{Cey} - J_{ey}\big|_{i+1/2,j,k}^{n-1/2}\omega_{Cex}\right)\omega_{Cey}\right] \\
&\qquad+ \frac{\Delta t\epsilon_0\tan\frac{\theta}{2}\sin\theta}{2|\omega_{Ce}|^2}\omega_{Pe}^2\left[\left(E_z\big|_{i+1/2,j,k}^{n}\omega_{Cex} - E_x\big|_{i+1/2,j,k}^{n}\omega_{Cez}\right)\omega_{Cez} - \left(E_x\big|_{i+1/2,j,k}^{n}\omega_{Cey} - E_y\big|_{i+1/2,j,k}^{n}\omega_{Cex}\right)\omega_{Cey}\right] \\
&\qquad- \frac{\Delta t\tan\frac{\theta}{2}\sin\theta}{2|\omega_{Ce}|^2}v_e\left[\left(J_{ez}\big|_{i+1/2,j,k}^{n-1/2}\omega_{Cex} - J_{ex}\big|_{i+1/2,j,k}^{n-1/2}\omega_{Cez}\right)\omega_{Cez} - \left(J_{ex}\big|_{i+1/2,j,k}^{n-1/2}\omega_{Cey} - J_{ey}\big|_{i+1/2,j,k}^{n-1/2}\omega_{Cex}\right)\omega_{Cey}\right].
\end{aligned} \tag{6}$$

*For the Corrector Step*:

$$\begin{aligned}
&J_{ex,c}\big|_{i+1/2,j,k}^{n+1/2} \\
&= J_{ex}\big|_{i+1/2,j,k}^{n-1/2} + \Delta t\epsilon_0\omega_{Pe}^2 E_x\big|_{i+1/2,j,k}^{n} - \Delta t v_e J_{ex,p}\big|_{i+1/2,j,k}^{n+1/2} - \frac{\sin\theta}{|\omega_{Ce}|}\left(J_{ey}\big|_{i+1/2,j,k}^{n-1/2}\omega_{Cez} - J_{ez}\big|_{i+1/2,j,k}^{n-1/2}\omega_{Cey}\right) \\
&\quad- \frac{\Delta t\epsilon_0\sin\theta}{2|\omega_{Ce}|}\omega_{Pe}^2\left(E_y\big|_{i+1/2,j,k}^{n}\omega_{Cez} - E_z\big|_{i+1/2,j,k}^{n}\omega_{Cey}\right) + \frac{\Delta t\sin\theta}{2|\omega_{Ce}|}v_e\left(J_{ey,p}\big|_{i+1/2,j,k}^{n+1/2}\omega_{Cez} - J_{ez,p}\big|_{i+1/2,j,k}^{n+1/2}\omega_{Cey}\right) \\
&\quad+ \frac{\tan\frac{\theta}{2}\sin\theta}{|\omega_{Ce}|^2}\left[\left(J_{ez}\big|_{i+1/2,j,k}^{n-1/2}\omega_{Cex} - J_{ex}\big|_{i+1/2,j,k}^{n-1/2}\omega_{Cez}\right)\omega_{Cez} - \left(J_{ex}\big|_{i+1/2,j,k}^{n-1/2}\omega_{Cey} - J_{ey}\big|_{i+1/2,j,k}^{n-1/2}\omega_{Cex}\right)\omega_{Cey}\right] \\
&\quad+ \frac{\Delta t\epsilon_0\tan\frac{\theta}{2}\sin\theta}{2|\omega_{Ce}|^2}\omega_{Pe}^2\left[\left(E_z\big|_{i+1/2,j,k}^{n}\omega_{Cex} - E_x\big|_{i+1/2,j,k}^{n}\omega_{Cez}\right)\omega_{Cez} - \left(E_x\big|_{i+1/2,j,k}^{n}\omega_{Cey} - E_y\big|_{i+1/2,j,k}^{n}\omega_{Cex}\right)\omega_{Cey}\right] \\
&\quad- \frac{\Delta t\tan\frac{\theta}{2}\sin\theta}{2|\omega_{Ce}|^2}v_e\left[\left(J_{ez,p}\big|_{i+1/2,j,k}^{n+1/2}\omega_{Cex} - J_{ex,p}\big|_{i+1/2,j,k}^{n+1/2}\omega_{Cez}\right)\omega_{Cez} - \left(J_{ex,p}\big|_{i+1/2,j,k}^{n+1/2}\omega_{Cey} - J_{ey,p}\big|_{i+1/2,j,k}^{n+1/2}\omega_{Cex}\right)\omega_{Cey}\right].
\end{aligned} \tag{7}$$

*E-Field Update*:

$$E_x\big|_{i+1/2,j,k}^{n+1} = E_x\big|_{i+1/2,j,k}^{n} + \frac{\Delta t}{\epsilon_0}\left[\frac{H_z\big|_{i+1/2,j+1/2,k}^{n+1/2} - H_z\big|_{i+1/2,j-1/2,k}^{n+1/2}}{\Delta y} - \frac{H_y\big|_{i+1/2,j,k+1/2}^{n+1/2} - H_y\big|_{i+1/2,j,k-1/2}^{n+1/2}}{\Delta z} - J_{ex}\big|_{i+1/2,j,k}^{n+1/2}\right]. \tag{8}$$

i.e., the electron density and the collision frequency, vary in the ionosphere according to solar activity (see [20]–[22]). Similarly, the Earth's magnetic field which extends from the Earth's interior out into space may also change over short-time scales (ms) due to disturbed currents in the ionosphere and over long-time scale (years) due to changes in the Earth's interior, particularly the iron-rich core [44]. The electron densities, collision frequencies, and geomagnetic field intensity, i.e., $B = |\mathbf{B}|$, are considered here as random variables, each having its own statistical distribution. This variation in the ionosphere structure and geomagnetic field impresses variation in the EM fields and current densities ($\mathbf{E}$, $\mathbf{H}$, and $\mathbf{J}_e$), which in turn are treated as output random variables. The exact distributions of the electron densities, the collision frequencies and the geomagnetic field intensities are unknown, so these input parameters are assumed to be characterized by a normal (Gaussian) or uniform probability distribution. For example, the electron density $n_e$, the collision frequency $v_e$, and the geomagnetic field intensity $B$ are defined by

$$\begin{cases} n_e(\xi_1) = \mu_{n_e} + \sigma_{n_e}\xi_1 \\ v_e(\xi_2) = \mu_{v_e} + \sigma_{v_e}\xi_2 \\ B(\xi_3) = \mu_B + \sigma_B\xi_3 \end{cases} \tag{9}$$

where $\mu_{n_e}$, $\mu_{v_e}$, and $\mu_B$ are the mean value of the parameters, $\sigma_{n_e}$, $\sigma_{v_e}$, and $\sigma_B$ are the standard deviation values, and $\xi_1$, $\xi_2$, and $\xi_3$ are independent normalized Gaussian random variables with a zero mean and unit standard deviation.

In order to implement the PCE method, the uncertain fields are expanded as an infinite summation of orthogonal basis functions $\psi_a(\boldsymbol{\xi})$. Similar to Taylor expansion, the infinite summation is often truncated to finite order $P$. For example,

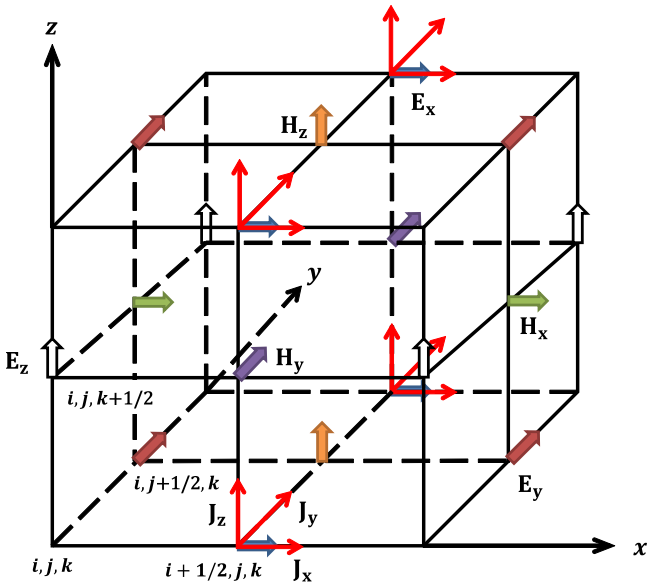


Fig. 1. Yee cell illustrating the spatial positioning of the magnetized plasma field components.

the $x$-components of the uncertain fields may be expressed as

$$H_x(x,y,z,t,\boldsymbol{\xi}) = \sum_{a=0}^{\infty} h_x^a(x,y,z,t)\psi_a(\boldsymbol{\xi}) \approx \sum_{a=0}^{P} \underbrace{h_x^a(x,y,z,t)}_{\text{deterministic}} \underbrace{\psi_a(\boldsymbol{\xi})}_{\text{stochastic}} \tag{10}$$

$$J_{ex}(x,y,z,t,\boldsymbol{\xi}) = \sum_{a=0}^{\infty} j_{ex}^a(x,y,z,t)\psi_a(\boldsymbol{\xi}) \approx \sum_{a=0}^{P} \underbrace{j_{ex}^a(x,y,z,t)}_{\text{deterministic}} \underbrace{\psi_a(\boldsymbol{\xi})}_{\text{stochastic}} \tag{11}$$

$$E_x(x,y,z,t,\boldsymbol{\xi}) = \sum_{a=0}^{\infty} e_x^a(x,y,z,t)\psi_a(\boldsymbol{\xi}) \approx \sum_{a=0}^{P} \underbrace{e_x^a(x,y,z,t)}_{\text{deterministic}} \underbrace{\psi_a(\boldsymbol{\xi})}_{\text{stochastic}} \tag{12}$$

where $h_x^a$, $j_{ex}^a$, and $e_x^a$ are the weighting coefficients, $\boldsymbol{\xi} = [\xi_1, \xi_2, \ldots, \xi_n]$ represents a vector containing an $n$ number of independent random variables, and $\psi$ are Hermite polynomials. By expanding the uncertain values in this manner, the dependence of the output fields on the random parameter $\boldsymbol{\xi}$ is separated from their dependence on time and spatial position. The choice of the orthogonal basis functions follows an Askey scheme to ensure optimal exponential convergence rate [25]. Here, Hermite polynomials are chosen due to the normal distribution of the random variables being considered in this case.

The total number of expansion terms is $(P+1)$ and is determined by

$$P+1 = \frac{(n+d)!}{n!d!} \tag{13}$$

where $d$ is the order of the highest order Hermite polynomial used in the expansion and $n$ is the number of random variables.

Upon choosing a proper basis, a numerical technique is needed to solve the coefficients $h_x^a$, $j_{ex}^a$, and $e_x^a$. This may be done either by repetitive executions or by modification of the existing deterministic solver. These two options are termed the collocation (nonintrusive) method and the Galerkin (intrusive) method, respectively. This paper focuses on the intrusive approach, since the Galerkin method typically offers more accurate and efficient solutions, even though it is more cumbersome to implement. The truncated expansions of the $H_x$, $J_{ex}$, and $E_x$ solutions and input data are substituted into the governing equations (5)–(8). A Galerkin projection is then used by successively evaluating the inner product of the expansion equations with each basis element $\psi_b(\boldsymbol{\xi})$, where $b = 0, \ldots, P$. Then, the orthogonality condition

$$\langle \psi_a(\boldsymbol{\xi}), \psi_b(\boldsymbol{\xi}) \rangle = \langle \psi_b^2(\boldsymbol{\xi}) \rangle \delta_{a,b} \tag{14}$$

is used where $\delta_{a,b}$ is the Kronecker delta function ($\delta_{a,b} = 0$ if $a \neq b$ and $\delta_{a,b} = 1$ if $a = b$). Utilizing this orthogonality condition yields a set of $P+1$ coupled deterministic equations as shown in (15) and (16) for the $H_x$-field and $E_x$-field updates, and in (17)–(18) for the $J_{ex}$-field updates, that can then be solved using the FDTD method

$$h_x^b\big|_{i,j+1/2,k+1/2}^{n+1/2} = h_x^b\big|_{i,j+1/2,k+1/2}^{n-1/2} + \frac{\Delta t}{\mu_0} \times \left[ \frac{e_y^b\big|_{i,j+1/2,k+1}^{n} - e_y^b\big|_{i,j+1/2,k}^{n}}{\Delta z} - \frac{e_z^b\big|_{i,j+1,k+1/2}^{n} - e_z^b\big|_{i,j,k+1/2}^{n}}{\Delta y} \right] \tag{15}$$

$$e_x^b\big|_{i+1/2,j,k}^{n+1} = e_x^b\big|_{i+1/2,j,k}^{n} + \frac{\Delta t}{\epsilon_0} \left[ \frac{h_z^b\big|_{i+1/2,j+1/2,k}^{n+1/2} - h_z^b\big|_{i+1/2,j-1/2,k}^{n+1/2}}{\Delta y} - \frac{h_y^b\big|_{i+1/2,j,k+1/2}^{n+1/2} - h_y^b\big|_{i+1/2,j,k-1/2}^{n+1/2}}{\Delta z} - j_{ex}^b\big|_{i+1/2,j,k}^{n+1/2} \right]. \tag{16}$$

Note that a standard (nonstochastic) FDTD simulation of plasma will calculate $H(x,y,z)$, $J_e(x,y,z)$, $E(x,y,z)$ at every time step, while a PCE-FDTD simulation will calculate $(P+1)$ weighting coefficients $h^a(x,y,z)$, $j_e^a(x,y,z)$, $e^a(x,y,z)$ $(a = 0, \ldots, P)$ at every time step. Therefore, if we are using $(P+1)$ polynomials to represent the stochastic problem, the coupling between coefficients will generate a system $(P+1)$ times larger. As a result, for the PCE-FDTD method, the memory consumption generally increases by a factor of $(P+1)$ and the simulation time increases approximately by a factor of $(P+1)^2$ than that of a standard (nonstochastic) FDTD simulation, since there are $(P+1)$ field

*For the Predictor Step*:

$$
\begin{aligned}
&j^{b}_{ex,p}\big|^{n+1/2}_{i+1/2,j,k} \\
&= j^{b}_{ex}\big|^{n-1/2}_{i+1/2,j,k} - \frac{1}{\langle\psi_b^2\rangle}\sum_{a=0}^{P}\left(\left\langle \sin\theta\frac{\omega_{Cez}}{|\omega_{Ce}|}\psi_a(\boldsymbol{\xi})\psi_b(\boldsymbol{\xi})\right\rangle j^{a}_{ey}\big|^{n-1/2}_{i+1/2,j,k} - \left\langle \sin\theta\frac{\omega_{Cey}}{|\omega_{Ce}|}\psi_a(\boldsymbol{\xi})\psi_b(\boldsymbol{\xi})\right\rangle j^{a}_{ez}\big|^{n-1/2}_{i+1/2,j,k}\right) \\
&\quad + \frac{1}{\langle\psi_b^2\rangle}\sum_{a=0}^{P}\left(\left\langle \tan\frac{\theta}{2}\sin\theta\frac{\omega_{Cez}\omega_{Cex}}{|\omega_{Ce}|^2}\psi_a(\boldsymbol{\xi})\psi_b(\boldsymbol{\xi})\right\rangle j^{a}_{ez}\big|^{n-1/2}_{i+1/2,j,k} - \left\langle \tan\frac{\theta}{2}\sin\theta\frac{\omega_{Cez}\omega_{Cez}}{|\omega_{Ce}|^2}\psi_a(\boldsymbol{\xi})\psi_b(\boldsymbol{\xi})\right\rangle j^{a}_{ex}\big|^{n-1/2}_{i+1/2,j,k}\right) \\
&\quad - \frac{1}{\langle\psi_b^2\rangle}\sum_{a=0}^{P}\left(\left\langle \tan\frac{\theta}{2}\sin\theta\frac{\omega_{Cey}\omega_{Cey}}{|\omega_{Ce}|^2}\psi_a(\boldsymbol{\xi})\psi_b(\boldsymbol{\xi})\right\rangle j^{a}_{ex}\big|^{n-1/2}_{i+1/2,j,k} - \left\langle \tan\frac{\theta}{2}\sin\theta\frac{\omega_{Cex}\omega_{Cey}}{|\omega_{Ce}|^2}\psi_a(\boldsymbol{\xi})\psi_b(\boldsymbol{\xi})\right\rangle j^{a}_{ey}\big|^{n-1/2}_{i+1/2,j,k}\right) \\
&\quad + \frac{\Delta t\epsilon_0}{\langle\psi_b^2\rangle}\sum_{a=0}^{P}\left[\left\langle \omega_{Pe}^2\psi_a(\boldsymbol{\xi})\psi_b(\boldsymbol{\xi})\right\rangle e^{a}_{x}\big|^{n}_{i+1/2,j,k} - \frac{1}{2}\left(\left\langle \omega_{Pe}^2\sin\theta\frac{\omega_{Cez}}{|\omega_{Ce}|}\psi_a(\boldsymbol{\xi})\psi_b(\boldsymbol{\xi})\right\rangle e^{a}_{y}\big|^{n}_{i+1/2,j,k}\right.\right. \\
&\qquad\qquad \left.\left. - \left\langle \omega_{Pe}^2\sin\theta\frac{\omega_{Cey}}{|\omega_{Ce}|}\psi_a(\boldsymbol{\xi})\psi_b(\boldsymbol{\xi})\right\rangle e^{a}_{z}\big|^{n}_{i+1/2,j,k}\right)\right] \\
&\quad + \frac{\Delta t\epsilon_0}{2\langle\psi_b^2\rangle}\sum_{a=0}^{P}\left(\left\langle \omega_{Pe}^2\tan\frac{\theta}{2}\sin\theta\frac{\omega_{Cez}\omega_{Cex}}{|\omega_{Ce}|^2}\psi_a(\boldsymbol{\xi})\psi_b(\boldsymbol{\xi})\right\rangle e^{a}_{z}\big|^{n}_{i+1/2,j,k} - \left\langle \omega_{Pe}^2\tan\frac{\theta}{2}\sin\theta\frac{\omega_{Cez}\omega_{Cez}}{|\omega_{Ce}|^2}\psi_a(\boldsymbol{\xi})\psi_b(\boldsymbol{\xi})\right\rangle e^{a}_{x}\big|^{n}_{i+1/2,j,k}\right) \\
&\quad - \frac{\Delta t\epsilon_0}{2\langle\psi_b^2\rangle}\sum_{a=0}^{P}\left(\left\langle \omega_{Pe}^2\tan\frac{\theta}{2}\sin\theta\frac{\omega_{Cey}\omega_{Cey}}{|\omega_{Ce}|^2}\psi_a(\boldsymbol{\xi})\psi_b(\boldsymbol{\xi})\right\rangle e^{a}_{x}\big|^{n}_{i+1/2,j,k} - \left\langle \omega_{Pe}^2\tan\frac{\theta}{2}\sin\theta\frac{\omega_{Cex}\omega_{Cey}}{|\omega_{Ce}|^2}\psi_a(\boldsymbol{\xi})\psi_b(\boldsymbol{\xi})\right\rangle e^{a}_{y}\big|^{n}_{i+1/2,j,k}\right) \\
&\quad + \frac{\Delta t}{\langle\psi_b^2\rangle}\sum_{a=0}^{P}\left[\langle \upsilon_e\psi_a(\boldsymbol{\xi})\psi_b(\boldsymbol{\xi})\rangle\, j^{a}_{ex}\big|^{n-1/2}_{i+1/2,j,k} - \frac{1}{2}\left(\left\langle \upsilon_e\sin\theta\frac{\omega_{Cez}}{|\omega_{Ce}|}\psi_a(\boldsymbol{\xi})\psi_b(\boldsymbol{\xi})\right\rangle j^{a}_{ey}\big|^{n-1/2}_{i+1/2,j,k}\right.\right. \\
&\qquad\qquad \left.\left. - \left\langle \upsilon_e\sin\theta\frac{\omega_{Cey}}{|\omega_{Ce}|}\psi_a(\boldsymbol{\xi})\psi_b(\boldsymbol{\xi})\right\rangle j^{a}_{ez}\big|^{n-1/2}_{i+1/2,j,k}\right)\right] \\
&\quad + \frac{\Delta t}{2\langle\psi_b^2\rangle}\sum_{a=0}^{P}\left(\left\langle \upsilon_e\tan\frac{\theta}{2}\sin\theta\frac{\omega_{Cez}\omega_{Cex}}{|\omega_{Ce}|^2}\psi_a(\boldsymbol{\xi})\psi_b(\boldsymbol{\xi})\right\rangle j^{a}_{ez}\big|^{n-1/2}_{i+1/2,j,k} - \left\langle \upsilon_e\tan\frac{\theta}{2}\sin\theta\frac{\omega_{Cez}\omega_{Cez}}{|\omega_{Ce}|^2}\psi_a(\boldsymbol{\xi})\psi_b(\boldsymbol{\xi})\right\rangle j^{a}_{ex}\big|^{n-1/2}_{i+1/2,j,k}\right) \\
&\quad - \frac{\Delta t}{2\langle\psi_b^2\rangle}\sum_{a=0}^{P}\left(\left\langle \upsilon_e\tan\frac{\theta}{2}\sin\theta\frac{\omega_{Cey}\omega_{Cey}}{|\omega_{Ce}|^2}\psi_a(\boldsymbol{\xi})\psi_b(\boldsymbol{\xi})\right\rangle j^{a}_{ex}\big|^{n-1/2}_{i+1/2,j,k} - \left\langle \upsilon_e\tan\frac{\theta}{2}\sin\theta\frac{\omega_{Cex}\omega_{Cey}}{|\omega_{Ce}|^2}\psi_a(\boldsymbol{\xi})\psi_b(\boldsymbol{\xi})\right\rangle j^{a}_{ey}\big|^{n-1/2}_{i+1/2,j,k}\right).
\end{aligned}
\tag{17}
$$

coefficients to solve for and each calculation requires the sum of the product of $(P+1)$ field coefficients with $(P+1)$ plasma inner products as shown in (17), as shown at the top of this page and (18), as shown at the top of the next page. Note that the simulation time needed for the $J$-fields calculations is longer than that of the $E$-fields and $H$-fields due to the higher complexity of the $J$-field update equations.

Here, all inner products should be precalculated for all $a, b = 0, \ldots, P$ using numerical integration. Note that the multivariate polynomial chaos basis functions are constructed from tensor products of the univariate polynomials as follows:

$$\psi_b(\boldsymbol{\xi}) = \prod_{i=1}^{n}\phi_{m_i^b}(\xi_i) \tag{19}$$

where $\phi_{m_i^b}(\xi_i)$ is a univariate orthogonal basis in $\xi_i$, and $m^b = [m_1^b, \ldots, m_n^b]$ is the multi-index of the polynomial $\psi_b$. Also, by using the multi-index definition and due to the statistical independence of the $\xi$'s, the multivariate triple/quadruple products may be determined from the univariate triple/quadruple products. For example,

$$
\begin{aligned}
&\langle \upsilon_e(\boldsymbol{\xi})\psi_b(\boldsymbol{\xi})\psi_c(\boldsymbol{\xi})\rangle \\
&\quad = \left\langle\left(\prod_{i=1}^{n}\upsilon_e^i(\xi_i)\right)\left(\prod_{i=1}^{n}\phi_{m_i^a}(\xi_i)\right)\left(\prod_{i=1}^{n}\phi_{m_i^b}(\xi_i)\right)\right\rangle \\
&\quad = \prod_{i=1}^{n}\left\langle \upsilon_e^i(\xi_i)\phi_{m_i^a}(\xi_i)\phi_{m_i^b}(\xi_i)\right\rangle
\end{aligned}
\tag{20}
$$

where $\upsilon_e^i = \mu_{\upsilon_e} + \sigma_{\upsilon_e}\xi_2$ with $i = 2$ and $\upsilon_e^i = 1$ with $i \neq 2$. Now, the calculation of these inner products must be performed only once. The statistics (mean, standard deviation, and variance) of the output fields may be calculated based on the results of the coefficients $e_u^a$, $h_u^a$, $j_u^a$ $(u = x, y, z)$. The $E_x$ field is provided as an example as

$$\mu[E_{x,i+1/2,j,k}(\boldsymbol{\xi})] = e^0_{x,i+1/2,j,k} \tag{21}$$

$$\sigma^2[E_{x,i+1/2,j,k}(\boldsymbol{\xi})] = \sum_{a=1}^{P}(e^a_{x,i+1/2,j,k})^2\langle\psi_a^2\rangle. \tag{22}$$

*For the Corrector Step*:

$$
\begin{aligned}
&j_{ex,c}^{b}\big|_{i+1/2,j,k}^{n+1/2} \\
&= j_{ex}^{b}\big|_{i+1/2,j,k}^{n-1/2} - \frac{1}{\langle\psi_b^2\rangle}\sum_{a=0}^{P}\left(\left\langle \sin\theta\frac{\omega_{Cez}}{|\omega_{Ce}|}\psi_a(\boldsymbol{\xi})\psi_b(\boldsymbol{\xi})\right\rangle j_{ey}^{a}\big|_{i+1/2,j,k}^{n-1/2} - \left\langle \sin\theta\frac{\omega_{Cey}}{|\omega_{Ce}|}\psi_a(\boldsymbol{\xi})\psi_b(\boldsymbol{\xi})\right\rangle j_{ez}^{a}\big|_{i+1/2,j,k}^{n-1/2}\right) \\
&\quad + \frac{1}{\langle\psi_b^2\rangle}\sum_{a=0}^{P}\left(\left\langle \tan\frac{\theta}{2}\sin\theta\frac{\omega_{Cez}\omega_{Cex}}{|\omega_{Ce}|^2}\psi_a(\boldsymbol{\xi})\psi_b(\boldsymbol{\xi})\right\rangle j_{ez}^{a}\big|_{i+1/2,j,k}^{n-1/2} - \left\langle \tan\frac{\theta}{2}\sin\theta\frac{\omega_{Cez}\omega_{Cex}}{|\omega_{Ce}|^2}\psi_a(\boldsymbol{\xi})\psi_b(\boldsymbol{\xi})\right\rangle j_{ex}^{a}\big|_{i+1/2,j,k}^{n-1/2}\right) \\
&\quad - \frac{1}{\langle\psi_b^2\rangle}\sum_{a=0}^{P}\left(\left\langle \tan\frac{\theta}{2}\sin\theta\frac{\omega_{Cey}\omega_{Cey}}{|\omega_{Ce}|^2}\psi_a(\boldsymbol{\xi})\psi_b(\boldsymbol{\xi})\right\rangle j_{ex}^{a}\big|_{i+1/2,j,k}^{n-1/2} - \left\langle \tan\frac{\theta}{2}\sin\theta\frac{\omega_{Cex}\omega_{Cey}}{|\omega_{Ce}|^2}\psi_a(\boldsymbol{\xi})\psi_b(\boldsymbol{\xi})\right\rangle j_{ey}^{a}\big|_{i+1/2,j,k}^{n-1/2}\right) \\
&\quad + \frac{\Delta t\epsilon_0}{\langle\psi_b^2\rangle}\sum_{a=0}^{P}\left[\left\langle \omega_{Pe}^2\psi_a(\boldsymbol{\xi})\psi_b(\boldsymbol{\xi})\right\rangle e_x^{a}\big|_{i+1/2,j,k}^{n} - \frac{1}{2}\left(\left\langle \omega_{Pe}^2\sin\theta\frac{\omega_{Cez}}{|\omega_{Ce}|}\psi_a(\boldsymbol{\xi})\psi_b(\boldsymbol{\xi})\right\rangle e_y^{a}\big|_{i+1/2,j,k}^{n}\right.\right. \\
&\qquad\qquad \left.\left. - \left\langle \omega_{Pe}^2\sin\theta\frac{\omega_{Cey}}{|\omega_{Ce}|}\psi_a(\boldsymbol{\xi})\psi_b(\boldsymbol{\xi})\right\rangle e_z^{a}\big|_{i+1/2,j,k}^{n}\right)\right] \\
&\quad + \frac{\Delta t\epsilon_0}{2\langle\psi_b^2\rangle}\sum_{a=0}^{P}\left(\left\langle \omega_{Pe}^2\tan\frac{\theta}{2}\sin\theta\frac{\omega_{Cez}\omega_{Cex}}{|\omega_{Ce}|^2}\psi_a(\boldsymbol{\xi})\psi_b(\boldsymbol{\xi})\right\rangle e_z^{a}\big|_{i+1/2,j,k}^{n} - \left\langle \omega_{Pe}^2\tan\frac{\theta}{2}\sin\theta\frac{\omega_{Cez}\omega_{Cez}}{|\omega_{Ce}|^2}\psi_a(\boldsymbol{\xi})\psi_b(\boldsymbol{\xi})\right\rangle e_x^{a}\big|_{i+1/2,j,k}^{n}\right) \\
&\quad - \frac{\Delta t\epsilon_0}{2\langle\psi_b^2\rangle}\sum_{a=0}^{P}\left(\left\langle \omega_{Pe}^2\tan\frac{\theta}{2}\sin\theta\frac{\omega_{Cey}\omega_{Cey}}{|\omega_{Ce}|^2}\psi_a(\boldsymbol{\xi})\psi_b(\boldsymbol{\xi})\right\rangle e_x^{a}\big|_{i+1/2,j,k}^{n} - \left\langle \omega_{Pe}^2\tan\frac{\theta}{2}\sin\theta\frac{\omega_{Cex}\omega_{Cey}}{|\omega_{Ce}|^2}\psi_a(\boldsymbol{\xi})\psi_b(\boldsymbol{\xi})\right\rangle e_y^{a}\big|_{i+1/2,j,k}^{n}\right) \\
&\quad + \frac{\Delta t}{\langle\psi_b^2\rangle}\sum_{a=0}^{P}\left[\langle \upsilon_e\psi_a(\boldsymbol{\xi})\psi_b(\boldsymbol{\xi})\rangle\, j_{ex,p}^{a}\big|_{i+1/2,j,k}^{n+1/2} - \frac{1}{2}\left(\left\langle \upsilon_e\sin\theta\frac{\omega_{Cez}}{|\omega_{Ce}|}\psi_a(\boldsymbol{\xi})\psi_b(\boldsymbol{\xi})\right\rangle j_{ey,p}^{a}\big|_{i+1/2,j,k}^{n+1/2}\right.\right. \\
&\qquad\qquad \left.\left. - \left\langle \upsilon_e\sin\theta\frac{\omega_{Cey}}{|\omega_{Ce}|}\psi_a(\boldsymbol{\xi})\psi_b(\boldsymbol{\xi})\right\rangle j_{ez,p}^{a}\big|_{i+1/2,j,k}^{n+1/2}\right)\right] \\
&\quad + \frac{\Delta t}{2\langle\psi_b^2\rangle}\sum_{a=0}^{P}\left(\left\langle \upsilon_e\tan\frac{\theta}{2}\sin\theta\frac{\omega_{Cez}\omega_{Cex}}{|\omega_{Ce}|^2}\psi_a(\boldsymbol{\xi})\psi_b(\boldsymbol{\xi})\right\rangle j_{ez,p}^{a}\big|_{i+1/2,j,k}^{n+1/2} - \left\langle \upsilon_e\tan\frac{\theta}{2}\sin\theta\frac{\omega_{Cez}\omega_{Cez}}{|\omega_{Ce}|^2}\psi_a(\boldsymbol{\xi})\psi_b(\boldsymbol{\xi})\right\rangle j_{ex,p}^{a}\big|_{i+1/2,j,k}^{n+1/2}\right) \\
&\quad - \frac{\Delta t}{2\langle\psi_b^2\rangle}\sum_{a=0}^{P}\left(\left\langle \upsilon_e\tan\frac{\theta}{2}\sin\theta\frac{\omega_{Cey}\omega_{Cey}}{|\omega_{Ce}|^2}\psi_a(\boldsymbol{\xi})\psi_b(\boldsymbol{\xi})\right\rangle j_{ex,p}^{a}\big|_{i+1/2,j,k}^{n+1/2} - \left\langle \upsilon_e\tan\frac{\theta}{2}\sin\theta\frac{\omega_{Cex}\omega_{Cey}}{|\omega_{Ce}|^2}\psi_a(\boldsymbol{\xi})\psi_b(\boldsymbol{\xi})\right\rangle j_{ey,p}^{a}\big|_{i+1/2,j,k}^{n+1/2}\right).
\end{aligned}
\tag{18}
$$

### C. Global Sensitivities

Global sensitivities are calculated to assess the relative impact of each input parameter on the output EM fields of the PCE plasma model. Sobol indices are widely used in this context [45]. It is straightforward to compute global sensitivity indices of the model response related to the input parameters with a minimum computational cost via PCE [46], [47]. The Sobol indices, for the output field $E_x$, and the set of inputs $u$ are given by [47]

$$S_u = \frac{\sum_{m\in K_u}\left(e_{x,i+1/2,j,k}^{m}\right)^2\langle\psi_m^2\rangle}{\sigma^2[E_{x,i+1/2,j,k}(\boldsymbol{\xi})]} \tag{23}$$

where $K_u$ is an index to the terms in (12) that contain $u$. For $n$ input variables, (23) yields $2^n-1$ indices and they all sum up to 1

$$\sum_{u\subseteq\{1,2,\ldots,n\}} S_u = \sum_{i=1}^{n} S_i + \sum_{1\le i<j\le n} S_{ij} + \cdots + S_{1,2,\ldots,n} = 1. \tag{24}$$

Since this number becomes quickly large when $n$ increases, and in order to avoid the need to consider too many sensitivity measures, in practice it is more useful to define the total indices [48], namely, $S_{T_i}$ (which express the total sensitivity of the variance of the output field $E_x$ due to each input variable $\xi_i$ alone and all its interactions with the other variables)

$$S_{T_i} = \sum_{u\ni i} S_u. \tag{25}$$

For example, in the case of three input parameters $n=3$, we have $S_{T_1} = S_1 + S_{1,2} + S_{1,3} + S_{1,2,3}$.

## III. Numerical Examples

The Galerkin-based PCE algorithm is now applied to examine uncertainty of 3-D EM wave propagation in magnetized cold plasma. A similar test as for the FDTD plasma model of [12] is used for the validation of the proposed algorithm. An $x$-polarized, $z$-directed Gaussian-pulsed plane wave (with no uncertainty in the source) is implemented to excite the

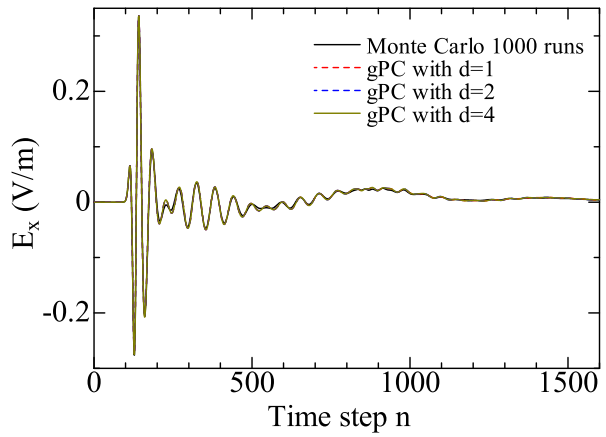


Fig. 2. Mean of $E_x$ for small input deviation case (observed at a point 40 cells away from the source).

FDTD grid. The first weighting coefficient of a source that has no uncertainty is just its mean value (i.e., the source waveform), and all of the other weighting coefficients are zero. This is written as

$$e^a_{x,source} = \begin{cases} \exp\left[\frac{-(t-50\Delta t)^2}{2(7\Delta t)^2}\right], & \text{if } a = 0 \\ 0, & \text{if } a > 0. \end{cases}$$

This is because the first weighting coefficient ($a = 0$) of a stochastic function represents its mean value. As a result, we only need to assign the first weighting coefficient to the source waveform and set the remaining weighting coefficients ($a > 0$) to zero. The lattice space increments in each Cartesian direction of the FDTD grid and the time step are $\Delta x = \Delta y = \Delta z = 1$ mm and $\Delta t = \Delta x/(c \times 0.55)$, respectively. In order to observe an effect of the plasma over a short distance for validation purposes, a large mean value of the magnetic field $B$ =0.06 T is applied to the plasma.

For validation, the input electron densities $n_e$, collision frequency $\upsilon_e$, and intensity of geomagnetic field $B$ for each simulation are first generated in a random manner with a normal distribution given by Table I (the standard deviation $\sigma$ in the Table I is defined by $\%\sigma/\mu$). These sets of data serve as inputs in Monte Carlo simulations to provide the actual statistical properties (mean and standard deviation values) of the output fields. Then, using the proposed PCE-based FDTD model, three separate simulation cases are run using Hermite polynomials of order $d = \{1, 2, 4\}$ to compare with the Monte Carlo results. Although in this paper we only study a normal distribution case as a numerical example, we find the same trend of the output, not shown, for the uniform distribution case.

Fig. 2 shows good agreement between the Monte Carlo and all three PCE FDTD model results for the mean electric field $E_x$ time-domain waveform as recorded 40 cells away from the source in the $z$-direction for the "small deviation" case of Table I. The corresponding standard deviations for each case are shown in Fig. 3. The results in Fig. 3 indicate that in the early time, an order higher than $d = 2$ does not yield much improvement in the standard deviation agreement between the PCE model results and the Monte Carlo results.

TABLE I
INPUT PARAMETERS AND UNCERTAINTY

| Case | Parameter | Mean value $\mu$ | Distribution |
|---|---|---|---|
| Small deviation | $n_e$ | $1.0\times10^{18}(m^{-3})$ | Gaussian, $\sigma = 2\%$ |
| | $v_e$ | $1.0\times10^{9}(1/s)$ | Gaussian, $\sigma = 6\%$ |
| | $B$ | 0.06 (T) | Gaussian, $\sigma = 4\%$ |
| Large deviation | $n_e$ | $1.0\times10^{18}(m^{-3})$ | Gaussian, $\sigma = 10\%$ |
| | $v_e$ | $1.0\times10^{9}(1/s)$ | Gaussian, $\sigma = 30\%$ |
| | $B$ | 0.06 (T) | Gaussian, $\sigma = 20\%$ |

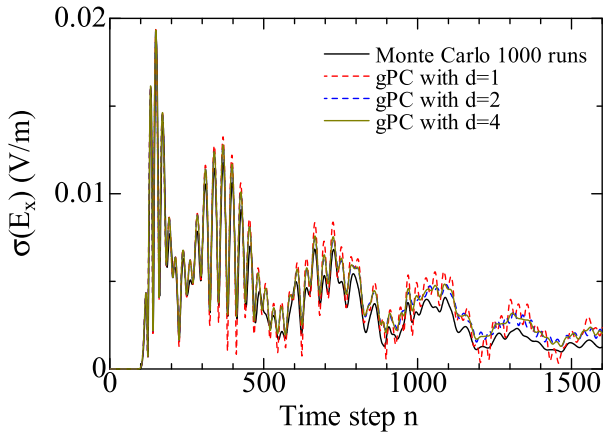


Fig. 3. Standard deviation of $E_x$ for small input deviation case (observed at a point 40 cells away from the source).

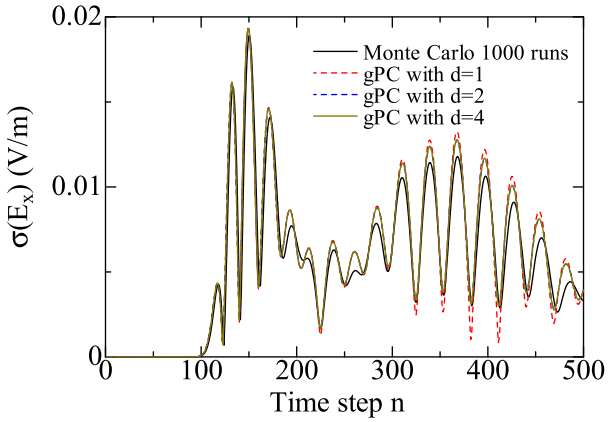


Fig. 4. Standard deviation of $E_x$ for small input deviation case at early time steps (observed at a point 40 cells away from the source).

This is highlighted in Fig. 4, which is a zoomed-in view of the early time results of Fig. 3. The $d = 2$ and $d = 4$ results in Fig. 3 are nearly identical, but the $d = 2$ case has the advantage of running faster than the $d = 4$ case. Finally, the late time results of Fig. 3 illustrate that the late-time results are improved by using a higher-order PCE model. As the order is increased, however, the simulation time increases and eventually can be as long or longer than all of the Monte Carlo simulations.

Next, Figs. 5 and 6 show the mean and standard deviation, respectively, of the electric field $E_x$ recorded 40 cells away from the source in the $z$-direction when the deviation of each input parameter is increased by a factor of 5, corresponding to the "large deviation" case of Table I. First, as would

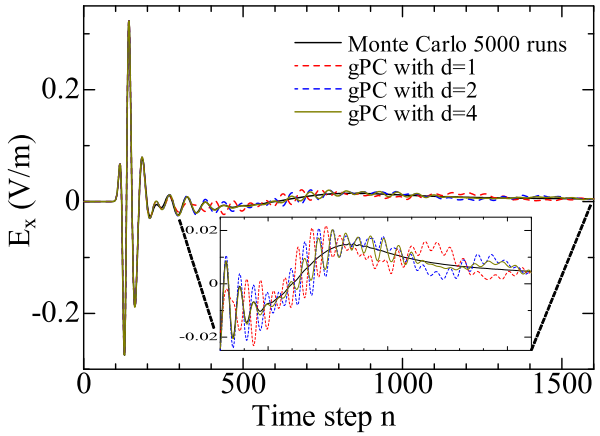


Fig. 5. Mean of $E_x$ for large input deviation case (observed at a point 40 cells away from the source). The zoomed-in view extends along the $x$-axis from 300 to 1600 time steps.

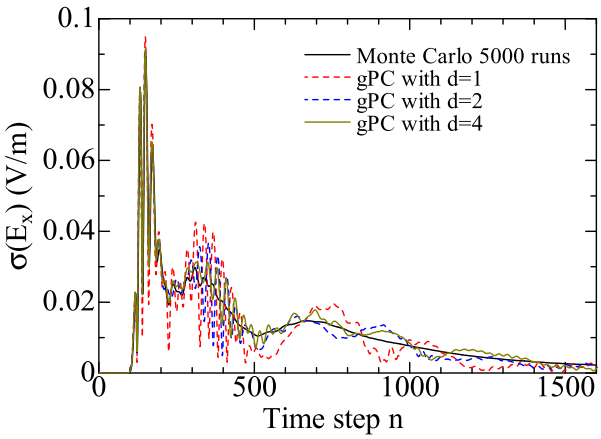


Fig. 6. Standard deviation of $E_x$ for large input deviation case (observed at a point 40 cells away from the source).

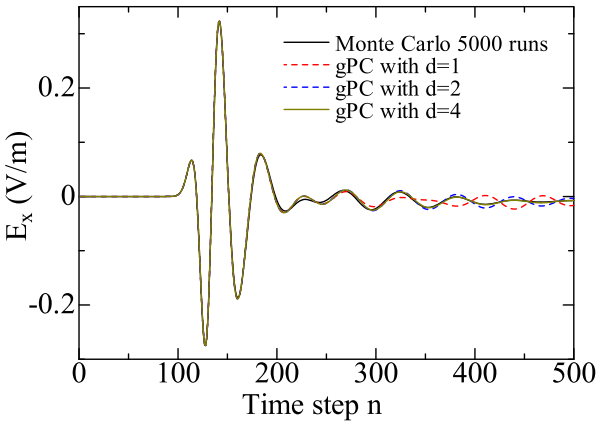


Fig. 7. Mean of $E_x$ for large input deviation case at early time steps (observed at a point 40 cells away from the source).

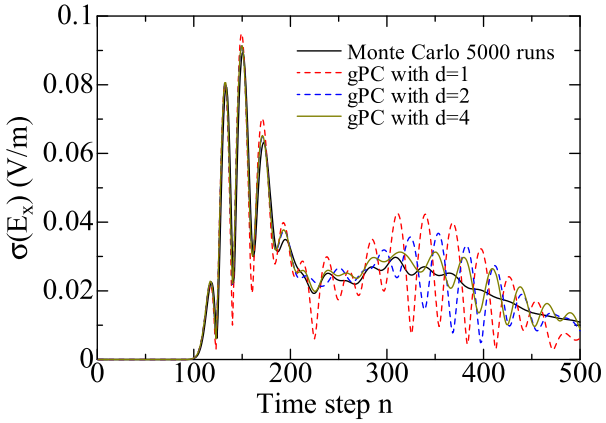


Fig. 8. Standard deviation of $E_x$ for large input deviation case at early time steps (observed at a point 40 cells away from the source).

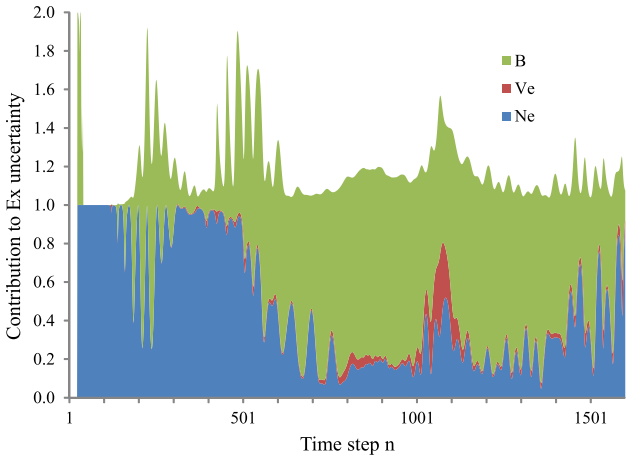


Fig. 9. Relative contribution of each input parameter to the uncertainty computed using the order $d = 4$ expansion for large input deviation case.

be expected, the standard deviation in Fig. 6 has a higher amplitude than the "small deviation" standard deviation of Fig. 3. More specifically, the results as shown in Figs. 2, 3, 5, and 6 indicate that the "small deviation" case results in a peak variation of 5.6% for the $E_x$-component, and the "large deviation" case results in a peak variation of 27.7% variation in $E_x$ (by comparing the peak mean value with the corresponding peak standard deviation value). Next, in the early time of Figs. 5 and 6, at least an order $d = 4$ is required for the mean and the standard deviation to agree well with the Monte Carlo results. This is better shown in Figs. 7 and 8, which are zoomed-in views of Figs. 5 and 6, respectively. This finding is similar to the Monte Carlo method wherein higher standard deviations require an increased number of Monte Carlo simulations to converge to the same level of error. However, for the PCE-based Galerkin approach, the accuracy depends on the order of the PCE (higher order leads to higher accuracy). Finally, as time progresses, higher order PCE simulations may be desirable in order to obtain better agreement with the Monte Carlo results. This should only be pursued when long-time spans are of interest, however, because the simulation time of the PCE models increases as the order is increased. We also note that the reason for the divergence of the PCE method after a short-time span is because the PCE method is known to fail for long-term integrations, losing its optimal convergence behavior [49]. A more efficient method, such as multielement PCE method [50], may be investigated to overcome this problem, i.e., in order to maintain an optimal

PCE when progressing to longer times. This is especially important for higher deviation problems.

Using the methodology of Section II-C, global sensitivities are calculated. Fig. 9 shows the relative contribution of each input parameter to the uncertainty in $E_x$ computed via (25). The uncertainty in $E_x$ is dominated by the electron density $n_e$ in the early time. The Gaussian pulse source used in the test case in this paper is expected to excite a lower frequency whistler mode wave after about 500 time steps, and this whistler mode travels along the Earth's magnetic field lines. Therefore, the uncertainty in the geomagnetic field $B$ has a greater impact during the later time steps. Also, the modeling results indicate that the collision frequency variations influence the propagating EM waves far less than the geomagnetic field and the electron density variations. This agrees with the observations in [51] and [52]. The figure also clearly demonstrates that the model is nonadditive and there is significant interactions between the parameters (as indicated by the contributions to the uncertainty extending above 1 on the $y$-axis). In other words, both the geomagnetic field and electron density are important, either when taken alone (i.e., first-order indices) or together (i.e., higher order indices). This may indicate that a higher order of the expansion in the PCE model and more Monte Carlo simulations may be required to improve accuracy of the results.

Table II compares the computational performance of the two methods. All simulations were performed on the Blue Waters supercomputer at the University of Illinois Urbana–Champaign using 1024 computational cores as well as identical time-step increments and grid sizes in order to obtain a fair comparison. As seen in Table II, the Monte Carlo method takes more than $10\times$ longer compared to the proposed PCE method in order to obtain reasonable agreement (comparing 1000 Monte Carlo simulations with the PCE simulation of order 2 for the "small

*For the Predictor Step*:

$$
\begin{aligned}
&j^b_{ex,p}\big|^{n+1/2}_{i+1/2,j,k} \\
&= j^b_{ex}\big|^{n-1/2}_{i+1/2,j,k} - \frac{\sin\theta}{|\omega_{Ce}|}\left(j^b_{ey}\big|^{n-1/2}_{i+1/2,j,k}\omega_{Cez} - j^b_{ez}\big|^{n-1/2}_{i+1/2,j,k}\omega_{Cey}\right) \\
&\quad + \frac{\tan\frac{\theta}{2}\sin\theta}{|\omega_{Ce}|^2}\left[\left(j^b_{ez}\big|^{n-1/2}_{i+1/2,j,k}\omega_{Cex} - j^b_{ex}\big|^{n-1/2}_{i+1/2,j,k}\omega_{Cez}\right)\omega_{Cez} - \left(j^b_{ex}\big|^{n-1/2}_{i+1/2,j,k}\omega_{Cey} - j^b_{ey}\big|^{n-1/2}_{i+1/2,j,k}\omega_{Cex}\right)\omega_{Cey}\right] \\
&\quad - \Delta t v_e\left\{ j^b_{ex}\big|^{n-1/2}_{i+1/2,j,k} - \frac{\sin\theta}{2|\omega_{Ce}|}\left(j^b_{ey}\big|^{n-1/2}_{i+1/2,j,k}\omega_{Cez} - j^b_{ez}\big|^{n-1/2}_{i+1/2,j,k}\omega_{Cey}\right) + \frac{\tan\frac{\theta}{2}\sin\theta}{2|\omega_{Ce}|^2}\right. \\
&\qquad \left.\times\left[\left(j^b_{ez}\big|^{n-1/2}_{i+1/2,j,k}\omega_{Cex} - j^b_{ex}\big|^{n-1/2}_{i+1/2,j,k}\omega_{Cez}\right)\omega_{Cez} - \left(j^b_{ex}\big|^{n-1/2}_{i+1/2,j,k}\omega_{Cey} - j^b_{ey}\big|^{n-1/2}_{i+1/2,j,k}\omega_{Cex}\right)\omega_{Cey}\right]\right\} \\
&\quad + \frac{\Delta t q_e^2}{m_e\langle\psi_b^2\rangle}\sum_{a=0}^{P}\langle n_e(\xi)\psi_a(\xi)\psi_b(\xi)\rangle\left\{ e^a_x\big|^n_{i+1/2,j,k} - \frac{\sin\theta}{2|\omega_{Ce}|}\left(e^a_y\big|^n_{i+1/2,j,k}\omega_{Cez} - e^a_z\big|^n_{i+1/2,j,k}\omega_{Cey}\right) + \frac{\tan\frac{\theta}{2}\sin\theta}{2|\omega_{Ce}|^2}\right. \\
&\qquad \left.\cdot\left[\left(e^a_z\big|^n_{i+1/2,j,k}\omega_{Cex} - e^a_x\big|^n_{i+1/2,j,k}\omega_{Cez}\right)\omega_{Cez} - \left(e^a_x\big|^n_{i+1/2,j,k}\omega_{Cey} - e^a_y\big|^n_{i+1/2,j,k}\omega_{Cex}\right)\omega_{Cey}\right]\right\} \qquad (26)
\end{aligned}
$$

*For the Corrector Step*:

$$
\begin{aligned}
&j^b_{ex,c}\big|^{n+1/2}_{i+1/2,j,k} \\
&= j^b_{ex}\big|^{n-1/2}_{i+1/2,j,k} - \frac{\sin\theta}{|\omega_{Ce}|}\left(j^b_{ey}\big|^{n-1/2}_{i+1/2,j,k}\omega_{Cez} - j^b_{ez}\big|^{n-1/2}_{i+1/2,j,k}\omega_{Cey}\right) \\
&\quad + \frac{\tan\frac{\theta}{2}\sin\theta}{|\omega_{Ce}|^2}\left[\left(j^b_{ez}\big|^{n-1/2}_{i+1/2,j,k}\omega_{Cex} - j^b_{ex}\big|^{n-1/2}_{i+1/2,j,k}\omega_{Cez}\right)\omega_{Cez} - \left(j^b_{ex}\big|^{n-1/2}_{i+1/2,j,k}\omega_{Cey} - j^b_{ey}\big|^{n-1/2}_{i+1/2,j,k}\omega_{Cex}\right)\omega_{Cey}\right] \\
&\quad - \Delta t v_e\left\{ j^b_{ex,p}\big|^{n+1/2}_{i+1/2,j,k} - \frac{\sin\theta}{2|\omega_{Ce}|}\left(j^b_{ey,p}\big|^{n+1/2}_{i+1/2,j,k}\omega_{Cez} - j^b_{ez,p}\big|^{n+1/2}_{i+1/2,j,k}\omega_{Cey}\right) + \frac{\tan\frac{\theta}{2}\sin\theta}{2|\omega_{Ce}|^2}\right. \\
&\qquad \left.\times\left[\left(j^b_{ez,p}\big|^{n+1/2}_{i+1/2,j,k}\omega_{Cex} - j^b_{ex,p}\big|^{n+1/2}_{i+1/2,j,k}\omega_{Cez}\right)\omega_{Cez} - \left(j^b_{ex,p}\big|^{n+1/2}_{i+1/2,j,k}\omega_{Cey} - j^b_{ey,p}\big|^{n+1/2}_{i+1/2,j,k}\omega_{Cex}\right)\omega_{Cey}\right]\right\} \\
&\quad + \frac{\Delta t q_e^2}{m_e\langle\psi_b^2\rangle}\sum_{a=0}^{P}\langle n_e(\xi)\psi_a(\xi)\psi_b(\xi)\rangle\left\{ e^a_x\big|^n_{i+1/2,j,k} - \frac{\sin\theta}{2|\omega_{Ce}|}\left(e^a_y\big|^n_{i+1/2,j,k}\omega_{Cez} - e^a_z\big|^n_{i+1/2,j,k}\omega_{Cey}\right) + \frac{\tan\frac{\theta}{2}\sin\theta}{2|\omega_{Ce}|^2}\right. \\
&\qquad \left.\cdot\left[\left(e^a_z\big|^n_{i+1/2,j,k}\omega_{Cex} - e^a_x\big|^n_{i+1/2,j,k}\omega_{Cez}\right)\omega_{Cez} - \left(e^a_x\big|^n_{i+1/2,j,k}\omega_{Cey} - e^a_y\big|^n_{i+1/2,j,k}\omega_{Cex}\right)\omega_{Cey}\right]\right\} \qquad (27)
\end{aligned}
$$

TABLE II
SIMULATION TIME REQUIRED BY THE MC AND THE PROPOSED PCE-BASED METHODS

| Method | Runs | Order $d$ | Cores | Simulation time |
|---|---|---|---|---|
| MC | 1000 | - | 1024 | 2 days 12 hours |
| MC | 5000 | - | 1024 | 12 days 12 hours |
| PCE | 1 | 1 | 1024 | 1 hour 03 mins |
| PCE | 1 | 2 | 1024 | 5 hours 51 mins |
| PCE | 1 | 4 | 1024 | 1 day 18 hours |

deviation" case, and 5000 Monte Carlo simulations with the PCE simulation of order 4 for the "large deviation" case).

Until this point, a general multivariate PCE method has been considered that involves the variability of three input parameters: the electron density, the collision frequency, and the geomagnetic field. For cases in which fewer variable input parameters are needed, the stochastic Lorentz equation for the predictor and corrector steps may be simplified. For example, when only electron density is modeled as an uncertain input parameter, then the equation reduces to the univariate random input parameter of the electron density as shown in (26) and (27), as shown at the bottom of the previous page. Accounting for only one random input variable (the electron density) greatly enhances the computational performance. For the PCE method, the memory consumption generally increases by a factor of $P + 1$ and the simulation time increases by a factor of $(P + 1)^2$.

## IV. CONCLUSION

The PCE Galerkin approach was developed and applied to uncertainty quantification of EM wave propagation in magnetized cold plasma. The statistical characteristics (mean and standard deviation) of the electric and magnetic fields were studied under the effect of geomagnetic field and ionosphere content (i.e., electron density and collision frequency) variability. The PCE FDTD results showed very good agreement with Monte Carlo results, especially in the early time results. In cases where late-time accuracy is needed, a higher order PCE model may be used. For the simulations in this paper, the PCE FDTD models ran more than $10\times$ faster than the corresponding Monte Carlo group of runs.

The tests of this paper involved relatively large values (high amplitude background magnetic field) in order to efficiently observe effects of the magnetized plasma on the propagating EM wave over a short distance. However, the geomagnetic field in the PCE FDTD model may be scaled in a straightforward manner to actual geomagnetic field amplitudes in order to model EM wave propagation in the Earth-ionosphere waveguide. It may therefore serve as an important tool for reliably estimating EM wave propagation in an uncertain / variable ionosphere, especially for large 3-D plasma scenarios wherein Monte Carlo simulations would be impractical to run.

## REFERENCES


[1] K. Yee, "Numerical solution of initial boundary value problems involving Maxwell's equations in isotropic media," *IEEE Trans. Antennas Propag.*, vol. AP-14, no. 3, pp. 302–307, May 1966.

[2] A. Taflove and S. C. Hagness, *Computational Electromagnetics: The Finite-Difference Time-Domain Method*, 3rd ed. Norwood, MA, USA: Artech House, 2005.

[3] J. P. Berenger, "Finite-difference computation of VLF-LF propagation in the Earth-ionosphere waveguide," in *Proc. EUROEM Symp.*, Bordeaux, France, May/Jun. 1994.

[4] S. A. Cummer, "Modeling electromagnetic propagation in the Earth-ionosphere waveguide," *IEEE Trans. Antennas Propag.*, vol. 48, no. 9, pp. 1420–1429, Sep. 2000.

[5] J. J. Simpson and A. Taflove, "Three-dimensional FDTD modeling of impulsive ELF propagation about the Earth-sphere," *IEEE Trans. Antennas Propag.*, vol. 52, no. 2, pp. 443–451, Feb. 2004.

[6] J. J. Simpson, "Current and future applications of 3-D global Earth-ionosphere models based on the full-vector Maxwell's equations FDTD method," *Surv. Geophys.*, vol. 30, no. 2, pp. 105–130, 2009.

[7] T. Otsuyama and M. Hayakawa, "FDTD simulation and experimental result on VLF scattering by ionospheric perturbations in Earth-ionosphere waveguide," *IEEJ Trans. Fundam. Mater.*, vol. 122, no. 1, pp. 59–63, 2002.

[8] H. Yang and V. P. Pasko, "Three-dimensional finite difference time domain modeling of the diurnal and seasonal variations in Schumann resonance parameters," *Radio Sci.*, vol. 41, no. 2, pp. 1–10, 2006.

[9] M. Thevenot, J. P. Bérenger, T. Monediere, and F. Jecko, "A FDTD scheme for the computation of VLF-LF propagation in the anisotropic Earth-ionosphere waveguide," *Ann. Telecommun.*, vol. 54, nos. 5–6, pp. 297–310, 1999.

[10] W. Hu and S. A. Cummer, "An FDTD model for low and high altitude lightning-generated EM fields," *IEEE Trans. Antennas Propag.*, vol. 54, no. 5, pp. 1513–1522, May 2006.

[11] Y. Yu, J. Niu, and J. J. Simpson, "A 3-D global Earth-ionosphere FDTD model including an anisotropic magnetized plasma ionosphere," *IEEE Trans. Antennas Propag.*, vol. 60, no. 7, pp. 3246–3256, Jul. 2012.

[12] Y. Yu and J. J. Simpson, "An E-J collocated 3-D FDTD model of electromagnetic wave propagation in magnetized cold plasma," *IEEE Trans. Antennas Propag.*, vol. 58, no. 2, pp. 469–478, Feb. 2010.

[13] A. Samimi and J. J. Simpson, "An efficient 3-D FDTD model of electromagnetic wave propagation in magnetized plasma," *IEEE Trans. Antennas Propag.*, vol. 63, no. 1, pp. 269–279, Jan. 2015.

[14] B. T. Nguyen, S. W. Vergara, C. D. Sarris, and J. J. Simpson, "Ionospheric variability effects on impulsive ELF antipodal propagation about the Earth-sphere," *IEEE Trans. Antennas Propag.*, vol. 66, no. 11, pp. 6244–6254, Nov. 2018.

[15] D. Bilitza, "International reference ionosphere 2000," *Radio Sci.*, vol. 36, no. 2, pp. 261–275, Mar./Apr. 2001.

[16] D. Bilitza and B. W. Reinisch, "International reference ionosphere 2007: Improvements and new parameters," *Adv. Space Res.*, vol. 42, no. 4, pp. 599–609, 2008.

[17] D. Bilitza, L.-A. McKinnell, B. Reinisch, and T. Fuller-Rowell, "The international reference ionosphere today and in the future," *J. Geodesy*, vol. 85, no. 12, pp. 909–920, 2011.

[18] D. Bilitza *et al.*, "The international reference ionosphere 2012—A model of international collaboration," *J. Space Weather Space Clim.*, vol. 4, Feb. 2014, Art. no. A07.

[19] J. M. Forbes, S. E. Palo, and X. Zhang, "Variability of the ionosphere," *J. Atmos. Sol. Terr. Phys.*, vol. 62, no. 8, pp. 685–693, 2000.

[20] P. G. Richards, "Seasonal and solar cycle variations of the ionospheric peak electron density: Comparison of measurement and models," *J. Geophys. Res.*, vol. 106, no. A7, pp. 12803–12819, 2001.

[21] J. S. Belrose and L. W. Hewitt, "Variation of collision frequency in the lowest ionosphere with solar activity," *Nature*, vol. 202, no. 4929, pp. 267–269, Apr. 1964.

[22] W. J. G. Beynon and E. S. O. Jones, "Collision frequency in the ionosphere and solar activity," *Nature*, vol. 203, no. 4950, p. 1159, 1964.

[23] B. T. Nguyen, C. Furse, and J. J. Simpson, "A 3-D stochastic FDTD model of electromagnetic wave propagation in magnetized ionosphere plasma," *IEEE Trans. Antennas Propag.*, vol. 63, no. 1, pp. 304–313, Jan. 2015.

[24] R. Ghanem and P. Spanos, *Stochastic Finite Element: A Spectral Approach*. New York, NY, USA: Springer-Verlag, 1991.

[25] D. B. Xiu and G. E. Karniadakis, "The Wiener–Askey polynomial chaos for stochastic differential equations," *SIAM J. Sci. Comput.*, vol. 24, no. 2, pp. 619–644, 2002.

[26] D. B. Xiu and G. E. Karniadakis, "Modeling uncertainty in flow simulations via generalized polynomial chaos," *J. Comput. Phys.*, vol. 187, no. 1, pp. 137–167, 2003.

[27] O. M. Knio and O. P. L. Maître, "Uncertainty propagation in CFD using polynomial chaos decomposition," *Fluid Dyn. Res.*, vol. 38, no. 9, p. 616, 2006.
[28] R. S. Edwards, A. C. Marvin, and S. J. Porter, "Uncertainty analyses in the finite-difference time-domain method," *IEEE Trans. Electromagn. Compat.*, vol. 52, no. 1, pp. 155–163, Feb. 2010.
[29] A. C. M. Austin, N. Sood, J. Siu, and C. D. Sarris, "Application of polynomial chaos to quantify uncertainty in deterministic channel models," *IEEE Trans. Antennas Propag.*, vol. 61, no. 11, pp. 5754–5761, Nov. 2013.
[30] A. C. M. Austin and C. D. Sarris, "Efficient analysis of geometrical uncertainty in the FDTD method using polynomial chaos with application to microwave circuits," *IEEE Trans. Microw. Theory Techn.*, vol. 61, no. 12, pp. 4293–4301, Dec. 2013.
[31] A. Biondi, D. V. Ginste, D. D. Zutter, P. Manfredi, and F. G. Canavero, "Variability analysis of interconnects terminated by general nonlinear loads," *IEEE Trans. Compon., Packag., Manuf. Technol.*, vol. 3, no. 7, pp. 1244–1251, Jul. 2013.
[32] F. Boeykens, H. Rogier, and L. Vallozzi, "An efficient technique based on polynomial chaos to model the uncertainty in the resonance frequency of textile antennas due to bending," *IEEE Trans. Antennas Propag.*, vol. 62, no. 3, pp. 1253–1260, Mar. 2014.
[33] C. Chauvière, J. S. Hesthaven, and L. Lurati, "Computational modeling of uncertainty in time-domain electromagnetics," *SIAM J. Sci. Comput.*, vol. 28, no. 2, pp. 751–775, 2006.
[34] H. Bagci, A. C. Yucel, J. S. Hesthaven, and E. Michielssen, "A fast stroud-based collocation method for statistically characterizing EMI/EMC phenomena on complex platforms," *IEEE Trans. Electromagn. Compat.*, vol. 51, no. 2, pp. 301–311, May 2009.
[35] D. Spina, F. Ferranti, T. Dhaene, L. Knockaert, G. Antonini, and D. V. Ginste, "Variability analysis of multiport systems via polynomial-chaos expansion," *IEEE Trans. Microw. Theory Techn.*, vol. 60, no. 8, pp. 2329–2338, Aug. 2012.
[36] P. Sumant, H. Wu, A. Cangellaris, and N. Aluru, "Reduced-order models of finite element approximations of electromagnetic devices exhibiting statistical variability," *IEEE Trans. Antennas Propag.*, vol. 60, no. 1, pp. 301–309, Jan. 2012.
[37] D. V. Ginste, D. D. Zutter, D. Deschrijver, T. Dhaene, P. Manfredi, and F. Canavero, "Stochastic modeling-based variability analysis of on-chip interconnects," *IEEE Trans. Compon., Packag., Manuf. Technol.*, vol. 2, no. 7, pp. 1182–1192, Jul. 2012.
[38] A. C. M. Austin, "Wireless channel characterization in burning buildings over 100–1000 MHz," *IEEE Trans. Antennas Propag.*, vol. 64, no. 7, pp. 3265–3269, Jul. 2016.
[39] B. T. Nguyen, A. Samimi, and J. J. Simpson, "A polynomial chaos approach for EM uncertainty propagation in 3D-FDTD magnetized cold plasma," in *Proc. IEEE Symp. Electromagn. Compat. Signal Integr.*, Santa Clara, CA, USA, Mar. 2015, pp. 1–5.
[40] J. P. Boris, *The Acceleration Calculation From a Scalar Potential*. Princeton, NJ, USA: Princeton University Plasma Physics Laboratory, 1970.
[41] C. K. Birdsall and A. B. Langdon, *Plasma Physics via Computer Simulation*. New York, NY, USA: Institute of Physics, 1991.
[42] G. A. Sod, "A survey of several finite difference methods for systems of nonlinear hyperbolic conservation laws," *J. Compat. Phys.*, vol. 27, no. 1, pp. 1–31, 1978.
[43] R. Garcia and R. A. Kahawita, "Numerical solution of the St. Venant equations with the MacCormack finite-difference scheme," *Int. J. Numer. Methods Fluids*, vol. 6, no. 5, pp. 259–274, 1986.
[44] J. Bloxham and D. Gubbins, "The secular variation of Earth's magnetic field," *Nature*, vol. 317, no. 6040, pp. 777–781, 1985.
[45] I. M. Sobol, "Global sensitivity indices for nonlinear mathematical models and their Monte Carlo estimates," *Math. Comput. Simul.*, vol. 55, nos. 1–3, pp. 271–280, 2001.
[46] B. Sudret, "Global sensitivity analysis using polynomial chaos expansions," *Rel. Eng. Syst. Saf.*, vol. 93, no. 7, pp. 964–979, 2008.
[47] T. Crestaux, O. Le Maître, and J.-M. Martinez, "Polynomial chaos expansion for sensitivity analysis," *Rel. Eng. Syst. Saf.*, vol. 94, no. 7, pp. 1161–1172, 2009.
[48] T. Homma and A. Saltelli, "Importance measures in global sensitivity analysis of nonlinear models," *Rel. Eng. Syst. Saf.*, vol. 52, no. 1, pp. 1–17, 1996.
[49] M. Gerritsma, J.-B. Van der Steen, P. Vos, and G. Karniadakis, "Time-dependent generalized polynomial chaos," *J. Comput. Phys.*, vol. 229, no. 22, pp. 8333–8363, 2010.
[50] X. Wan and G. E. Karniadakis, "An adaptive multi-element generalized polynomial chaos method for stochastic differential equations," *J. Comp. Phys.*, vol. 209, no. 2, pp. 617–642, 2005.
[51] K. Budden, *The Propagation Radio Waves*. New York, NY, USA: Cambridge Univ. Press, 1985.
[52] S. A. Cummer, U. S. Inan, and T. F. Bell, "Ionospheric D region remote sensing using VLF radio atmospherics," *Radio Sci.*, vol. 33, no. 6, pp. 1781–1792, 1998.

**Bach T. Nguyen** received the B.Eng. and M.Eng. degrees in electrical engineering from the National Defense Academy of Japan, Yokosuka, Japan, in 2007 and 2009, respectively, and the Ph.D. degree in electrical engineering from the University of Utah, Salt Lake City, UT, USA, in 2017.

His current research interests include computational electromagnetics, uncertainty quantification, RF/microwave technology, geophysics, plasma physics, and liquid crystal.

Dr. Nguyen was a recipient of the IEEE Antennas and Propagation Society (AP-S) Doctoral Research Award and the Honorable Mention in the Student Paper Competition of the 2014 IEEE AP-S International Symposium in Memphis, TN, USA.

**Alireza Samimi** received the B.S. degree in electrical engineering from Shiraz University, Shiraz, Iran, in 2005, the M.S. degree in electrical engineering from the University of Tabriz, Tabriz, Iran, in 2008, and the Ph.D. degree in electrical engineering from Virginia Tech, Blacksburg, VA, USA, in 2013.

Till 2015, he was with the Prof. Simpson's Computational Electrodynamics Laboratory, University of Utah, Salt Lake City, UT, USA, as a Post-Doctoral Fellow. He is currently a Senior Research Scientist with Nanometrics Inc., Milpitas, CA, USA. His current research interests include physics of the upper atmosphere, finite-difference time-domain solution of Maxwell's equations, and its applications in wave propagation in the Earth-ionosphere system.

**Stephen E. Wiechecki Vergara** (M'09) received the B.S. and M.S. degrees in mathematics from The University of Texas at San Antonio, San Antonio, TX, USA, in 1991 and 1993, respectively, the Ph.D. degree in statistical science from Southern Methodist University, Dallas, TX, USA, in 1998, and the M.S. degree in electrical engineering from the University of Central Florida, Orlando, FL, USA, in 2005.

He is currently the Director of Scientific Research/Analysis with Perspecta, Melbourne, FL, USA, where he oversees a team of scientists with diverse backgrounds in digital signal and image processing, statistics, machine learning, radar, electrooptics, computational electromagnetics, high-performance computing, and astrophysics.

**Costas D. Sarris** (SM'08) received the M.Sc. degree in applied mathematics and the Ph.D. degree in electrical engineering from the University of Michigan, Ann Arbor, MI, USA, in 2002.

He is currently a Full Professor and the Eugene V. Polistuk Chair in electromagnetic design with the Department of Electrical and Computer Engineering, University of Toronto, Toronto, ON, Canada. His current research interests include numerical electromagnetics, especially high-order, multiscale computational methods, modeling under stochastic uncertainty, and the applications of numerical methods to wireless channel modeling, wave propagation in complex media and metamaterials, wireless power transfer, and electromagnetic compatibility/interference problems.

Dr. Sarris was the TPC Chair for the 2015 IEEE AP-S International Symposium on Antennas and Propagation and CNC/USNC Joint Meeting and the TPC Vice Chair for the 2012 IEEE MTT-S International Microwave Symposium. He is the Chair of the MTT-S Technical Committee on Field Theory (MTT-15). He was a recipient of the IEEE MTT-S 2013 Outstanding Young Engineer Award. He was an Associate Editor of the IEEE TRANSACTIONS ON MICROWAVE THEORY AND TECHNIQUES from 2009 to 2013 and IEEE MICROWAVE AND WIRELESS COMPONENTS LETTERS from 2007 to 2009.

**Jamesina J. Simpson** (S'01–M'07–SM'12) received the B.S. and Ph.D. degrees in electrical engineering from Northwestern University, Evanston, IL, USA, in 2003 and 2007, respectively.

She is currently an Associate Professor with the Electrical and Computer Engineering Department, University of Utah, Salt Lake City, UT, USA. Her current research interests include the application of the full-vector Maxwell's equations finite-difference time-domain method to electromagnetic wave propagation spanning 15 orders of magnitude across the electromagnetic spectrum.

Dr. Simpson was a recipient of the 2010 National Science Foundation CAREER Award, the 2012 Donald G. Dudley, Jr. Undergraduate Teaching Award of the IEEE AP-S, and the Santimay Basu Medal from URSI in 2017.